Ravi Subrahmanyan
CSIRO-S&A, Curtin-CIRA
Jan 2022

An attempt at Stokes beamforming intra-station correlations in AAVS2 at 110 MHz

Executive Summary

This note reports on an attempt at polarisation calibration and imaging of intra-station correlations in SKA LOW station prototype AAVS2.

Visibilities in XX and YY correlations were modelled using embedded element patterns and a Global sky model + Sun, assuming the sky brightness in all sky pixels to be randomly polarised (unpolarised). Antenna-based complex gains versus time for X and Y polarisation receiver chains were solved for by comparing model with measured visibilities in XX and YY correlation products, respectively. These X and Y complex gain solutions were used to calibrate the XX, XY, YX and YY visibility correlations; XY phase remains uncalibrated.

Python scripts were written to combine the four correlation products and compute healpix sky images in Stokes parameters, while also correcting for embedded antenna-based voltage beam patterns that encode the direction-dependent responses of the polarised feeds. Snapshot images in Stokes I, Q, U and V are displayed at times when the Sun was at maximum elevation and when the Galactic Centre was close to zenith.

The fractional polarisations $(\sqrt{Q^2+U^2})/I$ and V/I appear to be small towards strong sources like the Sun and Galactic Centre at meridian crossing; however, the Stokes Q, U & V show systematic increase at large hour angles, and Stokes I deviates significantly from expected. Understanding the cause of this issue is work in progress.

Measurement set

The data are from an acquisition made during 21/22 April 2020 with the AAVS2 station, which consists of a 2D pseudo-random configuration of 256 SKALA4.1 antennas over a 38-m diameter ground area. Intrastation visibilities were recorded in a pair of adjacent 0.14-sec integrations and these pairs of snapshot observations were repeated every 5 mins over about 24 hours. The observations commenced in the evening of 21st April at about 1830 hrs local AWST time and ended 24 hrs later in the evening of 22nd April. The antenna signals were sampled at 800~MHz and channelised to give 512 coarse channels over 400 MHz. Digital data in a single coarse channel number 141, which has a noise equivalent width of 0.926 MHz centred at 110 MHz, was finely channelised over 32 frequency channels. Intra-station correlations were computed and recorded in these 32 fine frequency channels with 0.14-sec integration time.

At each integration time, all 32 channel data corresponding to each visibility correlation product were averaged together in frequency. Visibility pairs, with 0.14-sec integration and at adjacent times, were averaged together. Examination of the visibilities indicated that six of the 256 antennas were faulty and the data products involving those antennas were rejected. Thus the visibility data used in the analysis reported here consists of snapshot continuum visibility measurements, in XX, XY, YX and YY polarisations, in each of $250 \times (250-1)/2 = 31125$

baselines, spaced 5 minutes apart. The measurement data used here are initially “uncalibrated” in the sense that no prior bandpass or complex gain calibrations were applied to the intra-station correlations.

It may be noted here that X-polarisation in the SKALA4.1 antennas of the station are oriented EW and Y-polarisation is oriented NS.

Polarisation Calibration

The GDSM global sky model [Zheng et al. 2016] implemented in PyGSM was used to represent the sky as a healpix image. The Sun was added in at each timestamp assuming the flux density model in Benz [2009 Astronomy & Astrophysics, Vol. 4B, p.103] and computing its ephemeris sky position. The Sun was added in a pixel as a uniform brightness temperature of value corresponding to the flux density and resolution of the healpix representation. The sky model was assumed randomly polarised (unpolarised).

The beam models are from the EM simulation groups at Curtin-CIRA and INAF, using FEKO, which provide complex voltage patterns over sky azimuth-elevation, separately for each of X and Y feeds of each of the 256 embedded SKALA4.1 antennas in the AAVS2 station. The patterns of each of X and Y feeds in any antenna provides the complex voltage gain to vertical and horizontal sky polarisation. In principle, I expect that once the embedded element patterns (EEPs) are used in the measurement equation, and if they are accurate, there ought to be no residual “leakage terms” assuming that the electronics receiver chains are well isolated.

The visibility modelling is described in a Memo available at https://www.atnf.csiro.au/observers/memos/Modelling_Calibration_Imaging_intrastation_correlations_in_AAVS2_at_110_MHz.pdf in which Stokes I imaging was described. In brief, the model visibilities are computed, using a custom Python 3 script, for each AAVS2 baseline, at each timestamp corresponding to the measurement data, in XX and YY correlations, and taking into account the embedded element patterns (EEPs) for all antennas in the station. The Fourier transform was from curved healpix celestial sphere to 3D u, v, w visibility space.

MIRIAD task SELFCAL was used to solve for antenna based complex gains separately at each timestamp and in X and Y receiver chains. The model XX correlations were compared with measurement XX correlation to derive X gains, and similarly for Y gains.

The gain tables computed by MIRIAD SELFCAL provide complex gain values that measurements are to be multiplied by to get calibrated visibilities. All the four polarisation products — XX, XY, YX, YY — corresponding to each baseline and timestamp of the measurement data were calibrated using appropriate pairs of the X and Y receiver gains and using conjugates of the gains for the second antenna in the pair. No smoothing or interpolations of gain solutions were performed: gains computed independently at each timestamp were applied to correlations at that timestamp. XY phase remains uncalibrated.

Stokes Imaging using embedded beam patterns

The sky is represented by an all-sky healpix grid: a grid of pixel locations with fixed celestial coordinates on the celestial sphere. The imaging of polarisation products to Stokes sky pixels is performed as a two step process. First, at each time, the 4-vectors $[R_{XX}, R_{XY}, R_{YX}, R_{YY}]^T$ that represent visibility coherency in different baselines are transformed to direction-dependent Stokes

visibility vectors $[I_v, Q_v, U_v, V_v]^T$. Next, the Stokes visibilities are 3D Fourier transformed from u, v, w spatial frequency or visibility domain to the celestial sphere, to get Stokes intensities $[I, Q, U, V]^T$ at every healpix pixel. The first step accounts for the direction dependent gains of the embedded antennas; the second step accounts for the geometric delays. The polarisation imaging at each timestamp provides Stokes images at all sky pixels above horizon at that instant, corrected for the dissimilar EEP beams.

The linear dipole-like feeds of the SKALA4.1 antennas are connected to their respective receiver chains with a polarity that corresponds to the X-polarisation directed towards East and Y-polarisation towards North. The polarity is determined by which arm of the dipole connects to the signal terminal of the amplifier and which arm connects to ground: the eastern and northern arms of the dipoles are connected to amplifier input terminals and the western and southern arms are connected to amplifier grounds. The measured coherency vector $[R_{XX}, R_{XY}, R_{YX}, R_{YY}]^T$ corresponding to any baseline is determined by the E-field $[E_{1X}, E_{1Y}]^T$ at the terminals of one antenna along with the corresponding E-field $[E_{2X}, E_{2Y}]^T$ at the terminals of the second antenna. This measured coherency vector is the Kronecker product

$$\begin{bmatrix} R_{XX} \\ R_{XY} \\ R_{YX} \\ R_{YY} \end{bmatrix} = \begin{bmatrix} E_{1X} \\ E_{1Y} \end{bmatrix} \otimes \begin{bmatrix} E_{2X}^* \\ E_{2Y}^* \end{bmatrix}.$$

The FEKO EM modelling provides beam patterns using spherical convention with the horizontal component moving anti-clockwise from East to North and vertical component in the same convention as Zenith angle. I have transformed the frame of the complex patterns to horizontal H and vertical V polarisation components in every sky direction, assuming a convention that has the sky horizontal component H directed towards increasing Azimuth and vertical V component directed towards increasing Elevation. It may be noted here that Azimuth increases from North towards East. The complex gains of any antenna towards a sky direction thus defines a Jones matrix, which transforms the $[E_H, E_V]$ field incident from that sky direction to $[E_X, E_Y]$ voltages at the antenna terminals:

$$\begin{bmatrix} E_X \\ E_Y \end{bmatrix} = \begin{bmatrix} B_{X\phi} B_{X\theta} \\ B_{Y\phi} B_{Y\theta} \end{bmatrix} \begin{bmatrix} E_H \\ E_V \end{bmatrix}.$$

Here $B_{X\phi}$ and $B_{X\theta}$ represent the complex beam response of the X polarisation feed of the antenna to horizontal and vertical polarisation components, respectively, of the incident field. Similarly, $B_{Y\phi}$ and $B_{Y\theta}$ represent complex beam response of Y polarisation of the antenna to horizontal and vertical polarisation components, respectively, of the incident field. These are the beam patterns computed in EM simulations and whether they are used directly or their complex conjugates are used depends on the sign of the exponent in the Fourier transform from visibility domain to celestial sphere, which is simply decided by convention. I have found that for the convention adopted in acquisition of the measurement data, complex conjugates of the FEKO model beam patterns are to be used for transforming fields from celestial sphere to visibility domain.

The average complex antenna patterns are shown in Figs. 1 & 2 in the following page: amplitudes and phases are shown separately. These are averages over the 256 embedded element patterns

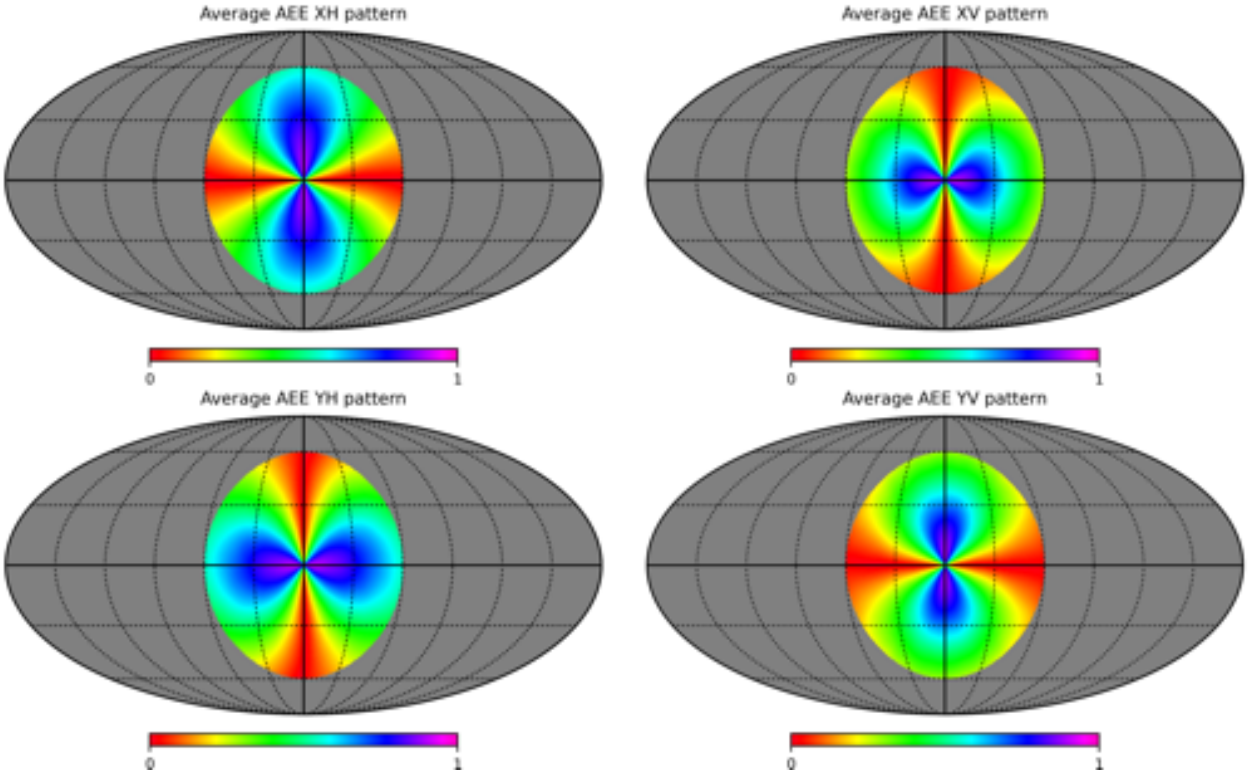

Figure 1 above shows the amplitudes of the average embedded element patterns, limited to elevations above 30 degrees. The images are in sky projection with North upwards, East to the left and zenith at the centre.

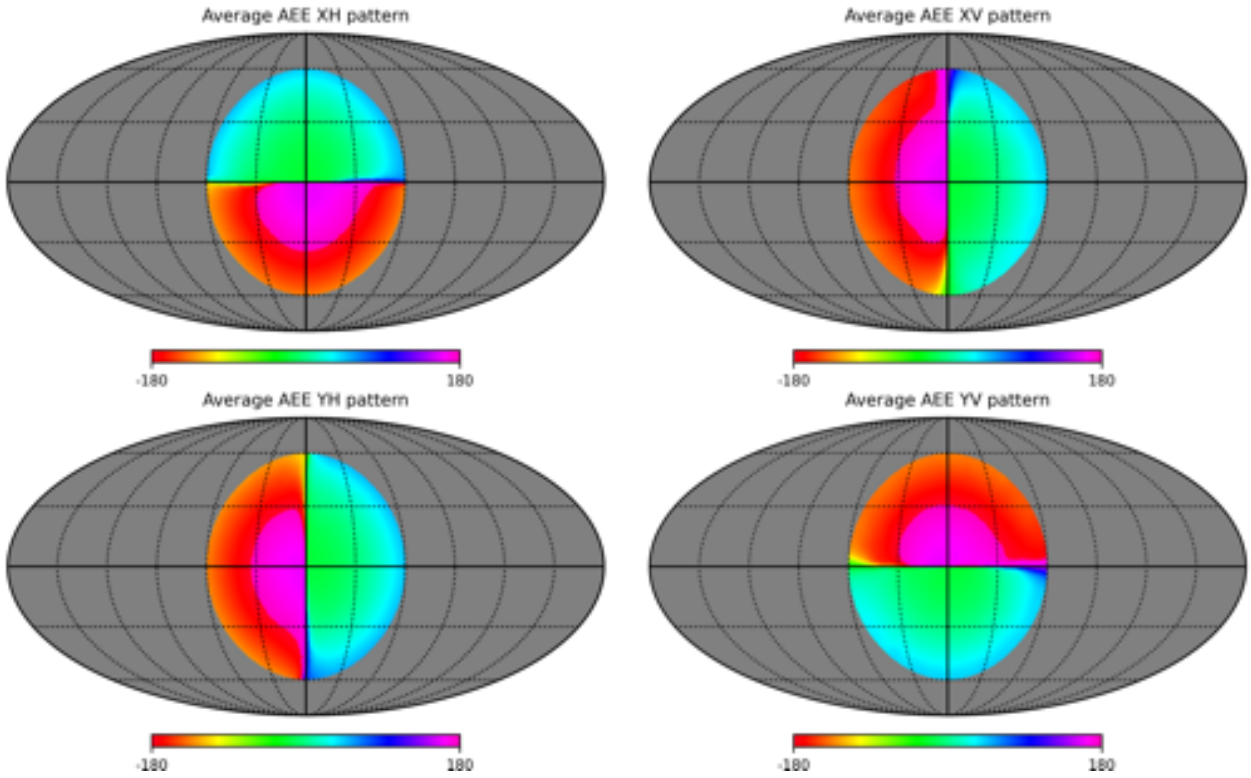

Figure 2 above shows the phase of the average embedded element patterns.

and not the patterns for an isolated antenna.

In any sky direction, the incident E-fields $[E_{1H}, E_{2V}]$ and $[E_{2H}, E_{2V}]$ determine the coherency vector $[R_{HH}, R_{HV}, R_{VH}, R_{VV}]$ in the *H-V* frame tangent to the celestial sphere. The coherency vector is, once again, a Kronecker product:

$$\begin{bmatrix} R_{HH} \\ R_{HV} \\ R_{VH} \\ R_{VV} \end{bmatrix} = \begin{bmatrix} E_{1H} \\ E_{1V} \end{bmatrix} \otimes \begin{bmatrix} E^*_{2H} \\ E^*_{2V} \end{bmatrix}.$$

In any baseline, the coherency vector that is described in the *H-V* frame towards a sky direction may be transformed to a coherency vector that is described in the *X-Y* reference frame at the antenna terminals. The 4×4 matrix that describes this transformation is the Kronecker product of the Jones matrices describing the complex antenna beam patterns:

$$\begin{bmatrix} R_{XX} \\ R_{XY} \\ R_{YX} \\ R_{YY} \end{bmatrix} = \left(\begin{bmatrix} B_{1X\phi} B_{1X\theta} \\ B_{1Y\phi} B_{1Y\theta} \end{bmatrix} \otimes \begin{bmatrix} B^*_{2X\phi} B^*_{2X\theta} \\ B^*_{2Y\phi} B^*_{2Y\theta} \end{bmatrix} \right) \begin{bmatrix} R_{HH} \\ R_{HV} \\ R_{VH} \\ R_{VV} \end{bmatrix}.$$

In any sky direction and in the *H-V* frame towards that sky direction, the transformation of a Stokes visibility vector $[I'_v, Q'_v, U'_v, V'_v]^T$ to a coherency vector $[R_{HH}, R_{HV}, R_{VH}, R_{VV}]^T$ is described by the matrix operation:

$$\begin{bmatrix} R_{HH} \\ R_{HV} \\ R_{VH} \\ R_{VV} \end{bmatrix} = \begin{bmatrix} 1 & 1 & 0 & 0 \\ 0 & 0 & 1 & j \\ 0 & 0 & 1 & -j \\ 1 & -1 & 0 & 0 \end{bmatrix} \begin{bmatrix} I'_v \\ Q'_v \\ U'_v \\ V'_v \end{bmatrix}.$$

The Stokes intensities in any sky direction are, by convention, defined in a (χ, ψ) reference plane tangent to the celestial sphere that has χ axis locally towards North and ψ axis towards East. The right-handed coordinate system (χ, ψ, ω) at that location on the celestial sphere would have the positive of the third axis ω towards the observer. This is the cartesian referential defined by the International Astronomical Union [IAU, 1974, Transactions of the IAU Vol. 15B (1973) 166].

Towards any sky direction or position on the celestial sphere, the parallactic angle q is the position angle of zenith. This position angle at any position on the celestial sphere is, by definition, measured counterclockwise from North towards East, which is the angle measured counterclockwise from χ towards ψ. The vertical *V* axis of the (H, V) frame is towards zenith; therefore, rotation of the (χ, ψ) axes to (H, V) is a clockwise rotation through angle $(q - \pi/2)$ when viewed along the direction of propagation.

Imaging Method A

Computationally, the simplest implementation of rotation between the above IAU convention and the (H, V) frame is in the celestial sphere, where the 4-vector of Stokes intensities may be rotated; this is reasonable for snapshot imaging and for compact arrays where the parallactic angle for a sky pixel is the same as seen from all antennas. Thus for snapshot visibilities of AAVS2, we may adopt the measurement equation:

$$\begin{bmatrix} R_{XX} \\ R_{XY} \\ R_{YX} \\ R_{YY} \end{bmatrix} = \left(\begin{bmatrix} B_{1X\phi} B_{1X\theta} \end{bmatrix} \otimes \begin{bmatrix} B^*_{2X\phi} B^*_{2X\theta} \end{bmatrix} \right) \begin{bmatrix} 1 & 1 & 0 & 0 \\ 0 & 0 & 1 & j \\ 0 & 0 & 1 & -j \\ 1 & -1 & 0 & 0 \end{bmatrix} \begin{bmatrix} I'_v \\ Q'_v \\ U'_v \\ V'_v \end{bmatrix}.$$

In the custom Python script, the matrix for the transformation from $[I'_v, Q'_v, U'_v, V'_v]^T$ to $[R_{XX}, R_{XY}, R_{YX}, R_{YY}]^T$ is computed for each baseline and for each sky direction, using the embedded beam patterns for the pair of antennas forming the baseline. The calibrated coherency vector $[R_{XX}, R_{XY}, R_{YX}, R_{YY}]^T$ for each baseline is then matrix multiplied by the matrix inverse of this transformation matrix, to give the Stokes visibility vector $[I'_v, Q'_v, U'_v, V'_v]^T$ for that baseline, in the (H, V) frame for that sky direction.

At each timestamp, the Stokes visibilities $[I'_v, Q'_v, U'_v, V'_v]^T$ in (u, v, w) visibility domain are then 3D Fourier transformed to the celestial sphere, using the Fourier transform kernel

$$e^{-2\pi(ul+vm+wn)}.$$

The Fourier transformation yields Stokes intensity vectors $[I', Q', U', V']^T$ at (l, m, n) coordinates of sky pixels.

The minus sign in the exponent is chosen to be consistent with the convention in the computation of coherency vectors in the AAVS2 correlator (at least for the 21/22 April 2020 dataset). As mentioned above, for this adopted sign convention, the complex EM beam models provided by the EM simulations group need to be conjugated and then used as the terms $B_{X\phi}, B_{X\theta}, B_{Y\phi},$ and $B_{Y\theta}$ in the Jones matrices for the transformation.

In each sky direction, the Stokes intensity vector $[I', Q', U', V']^T$ is summed over all baselines and finally a direction-dependent rotation

$$\begin{bmatrix} I \\ Q \\ U \\ V \end{bmatrix} = \begin{bmatrix} 1 & 0 & 0 & 0 \\ 0 & cos(2q-\pi) & -sin(2q-\pi) & 0 \\ 0 & sin(2q-\pi) & cos(2q-\pi) & 0 \\ 0 & 0 & 0 & 1 \end{bmatrix} \begin{bmatrix} I' \\ Q' \\ U' \\ V' \end{bmatrix}$$

is made to get Stokes intensities $[I, Q, U, V]^T$ at all sky pixels in the (χ, ψ) frame. This yields Stokes intensities in the cartesian referential defined by the IAU.

Imaging Method B

In Earth-rotation synthesis imaging, where parallactic angles of sky pixels change over time and hence for different records of the measurement set, the Stokes intensities on the celestial sphere are Fourier transformed to the visibility domain, and the Stokes coherency vectors are then rotated from IAU (χ, ψ) frame to (H, V) frame in individual baselines using the parallactic angles appropriate for the sky pixel at the visibility timestamp. Of course, this assumes that the array is compact and the parallactic angle for a sky pixel is the same as seen from all antennas, which is a reasonable assumption for AAVS2.

$[I'_v, Q'_v, U'_v, V'_v]^T$ is the Stokes visibility vector in the (H, V) frame. If we denote the corresponding Stokes visibility vector in the (χ, ψ) frame to be $[I_v, Q_v, U_v, V_v]^T$, then

$$\begin{bmatrix} I'_v \\ Q'_v \\ U'_v \\ V'_v \end{bmatrix} = \begin{bmatrix} 1 & 0 & 0 & 0 \\ 0 & cos(2q-\pi) & sin(2q-\pi) & 0 \\ 0 & -sin(2q-\pi) & cos(2q-\pi) & 0 \\ 0 & 0 & 0 & 1 \end{bmatrix} \begin{bmatrix} I_v \\ Q_v \\ U_v \\ V_v \end{bmatrix}.$$

Putting it all together, the transformation from Stokes visibilities in IAU frame to coherency vector in antenna coordinates is

$$\begin{bmatrix} R_{XX} \\ R_{XY} \\ R_{YX} \\ R_{YY} \end{bmatrix} = \left(\begin{bmatrix} B_{1X\phi}B_{1X\theta} \\ B_{1Y\phi}B_{1Y\theta} \end{bmatrix} \otimes \begin{bmatrix} B^*_{2X\phi}B^*_{2X\theta} \\ B^*_{2Y\phi}B^*_{2Y\theta} \end{bmatrix} \right) \begin{bmatrix} 1 & 1 & 0 & 0 \\ 0 & 0 & 1 & j \\ 0 & 0 & 1 & -j \\ 1 & -1 & 0 & 0 \end{bmatrix} \begin{bmatrix} 1 & 0 & 0 & 0 \\ 0 & cos(2q-\pi) & sin(2q-\pi) & 0 \\ 0 & -sin(2q-\pi) & cos(2q-\pi) & 0 \\ 0 & 0 & 0 & 1 \end{bmatrix} \begin{bmatrix} I_v \\ Q_v \\ U_v \\ V_v \end{bmatrix}.$$

The matrices for field rotation and conversion from Stokes coherency vector to the coherency vector $[R_{HH}, R_{HV}, R_{VH}, R_{VV}]^T$ may be combined:

$$\begin{bmatrix} R_{XX} \\ R_{XY} \\ R_{YX} \\ R_{YY} \end{bmatrix} = \left(\begin{bmatrix} B_{1X\phi}B_{1X\theta} \\ B_{1Y\phi}B_{1Y\theta} \end{bmatrix} \otimes \begin{bmatrix} B^*_{2X\phi}B^*_{2X\theta} \\ B^*_{2Y\phi}B^*_{2Y\theta} \end{bmatrix} \right) \begin{bmatrix} 1 & cos(2q-\pi) & sin(2q-\pi) & 0 \\ 0 & -sin(2q-\pi) & cos(2q-\pi) & j \\ 0 & -sin(2q-\pi) & cos(2q-\pi) & -j \\ 1 & -cos(2q-\pi) & -sin(2q-\pi) & 0 \end{bmatrix} \begin{bmatrix} I_v \\ Q_v \\ U_v \\ V_v \end{bmatrix}.$$

In the custom Python script, the matrix for the transformation from $[I_v, Q_v, U_v, V_v]^T$ to $[R_{XX}, R_{XY}, R_{YX}, R_{YY}]^T$ is computed for each baseline and for each sky direction, using the embedded beam patterns for the pair of antennas forming the baseline. The calibrated coherency vector $[R_{XX}, R_{XY}, R_{YX}, R_{YY}]^T$ for each baseline is then matrix multiplied by the matrix inverse of this transformation matrix, to give the Stokes visibility vector $[I_v, Q_v, U_v, V_v]^T$ for that baseline, in the (χ, ψ) frame for that sky direction.

Finally, the Stokes visibilities are Fourier transformed and accumulated in the celestial healpix sky pixels using the Fourier transform kernel:

$$e^{-2\pi(ul+vm+wn)}.$$

The Fourier transformation now directly yields Stokes intensity vectors $[I, Q, U, V]^T$ in IAU frame.

This is the implementation in MIRIAD (see https://www.atnf.csiro.au/computing/software/miriad/userguide/node74.html) for rotation of feeds with respect to sky over the synthesis observation.

Imaging Method C

A third and more exact formulation is to treat the field rotation for the i-th antenna as a direction dependent Jones matrix:

$$\begin{bmatrix} E_{iH} \\ E_{iV} \end{bmatrix} = \begin{bmatrix} sin(q_i) & -cos(q_i) \\ cos(q_i) & sin(q_i) \end{bmatrix} \begin{bmatrix} E_{i\chi} \\ E_{i\psi} \end{bmatrix}$$

that transforms the incident EM wave components in IAU (χ, ψ) frame to EM wave components in (H, V) frame.

Combining the Jones matrices for beam patterns with the above Jones matrix for field rotation:

$$\begin{bmatrix} E_{iX} \\ E_{iY} \end{bmatrix} = \begin{bmatrix} B_{iX\phi}B_{iX\theta} \\ B_{iY\phi}B_{iY\theta} \end{bmatrix} \begin{bmatrix} sin(q_i) & -cos(q_i) \\ cos(q_i) & sin(q_i) \end{bmatrix} \begin{bmatrix} E_{i\chi} \\ E_{i\psi} \end{bmatrix}$$

The coherency vector for any baseline from antenna 1 to antenna 2 may be written as

$$\begin{bmatrix} R_{XX} \\ R_{XY} \\ R_{YX} \\ R_{YY} \end{bmatrix} = \left\{ \begin{bmatrix} B_{1X\phi}B_{1X\theta} \\ B_{1Y\phi}B_{1Y\theta} \end{bmatrix} \begin{bmatrix} sin(q_1) & -cos(q_1) \\ cos(q_1) & sin(q_1) \end{bmatrix} \begin{bmatrix} E_{1\chi} \\ E_{1\psi} \end{bmatrix} \right\} \otimes \left\{ \begin{bmatrix} B_{2X\phi}B_{2X\theta} \\ B_{2Y\phi}B_{2Y\theta} \end{bmatrix} \begin{bmatrix} sin(q_2) & -cos(q_2) \\ cos(q_2) & sin(q_2) \end{bmatrix} \begin{bmatrix} E_{2\chi} \\ E_{2\psi} \end{bmatrix} \right\}$$

$$= \left\{ \begin{bmatrix} B_{1X\phi}B_{1X\theta} \\ B_{1Y\phi}B_{1Y\theta} \end{bmatrix} \otimes \begin{bmatrix} B_{2X\phi}B_{2X\theta} \\ B_{2Y\phi}B_{2Y\theta} \end{bmatrix} \right\} \left\{ \begin{bmatrix} sin(q_1) & -cos(q_1) \\ cos(q_1) & sin(q_1) \end{bmatrix} \otimes \begin{bmatrix} sin(q_2) & -cos(q_2) \\ cos(q_2) & sin(q_2) \end{bmatrix} \right\} \begin{bmatrix} R_{\chi\chi} \\ R_{\chi\psi} \\ R_{\psi\chi} \\ R_{\psi\psi} \end{bmatrix}$$

$$= \left\{ \begin{bmatrix} B_{1X\phi}B_{1X\theta} \\ B_{1Y\phi}B_{1Y\theta} \end{bmatrix} \otimes \begin{bmatrix} B_{2X\phi}B_{2X\theta} \\ B_{2Y\phi}B_{2Y\theta} \end{bmatrix} \right\} \left\{ \begin{bmatrix} sin(q_1) & -cos(q_1) \\ cos(q_1) & sin(q_1) \end{bmatrix} \otimes \begin{bmatrix} sin(q_2) & -cos(q_2) \\ cos(q_2) & sin(q_2) \end{bmatrix} \right\} \begin{bmatrix} 1 & 1 & 0 & 0 \\ 0 & 0 & 1 & j \\ 0 & 0 & 1 & -j \\ 1 & -1 & 0 & 0 \end{bmatrix} \begin{bmatrix} I_v \\ Q_v \\ U_v \\ V_v \end{bmatrix}$$

where q_1 and q_2 are the parallactic angles of the sky pixel as viewed from antennas 1 and 2.

In the custom Python script, the matrix for the transformation from $[I_v, Q_v, U_v, V_v]^T$ to $[R_{XX}, R_{XY}, R_{YX}, R_{YY}]^T$ is computed for each baseline and for each sky direction, using the embedded beam patterns for the pair of antennas forming the baseline. The calibrated coherency vector $[R_{XX}, R_{XY}, R_{YX}, R_{YY}]^T$ for each baseline is then matrix multiplied by the matrix inverse of this transformation matrix, to give the Stokes visibility vector $[I_v, Q_v, U_v, V_v]^T$ for that baseline, in the IAU (χ, ψ) frame for that sky direction.

Finally, the Stokes visibilities are Fourier transformed and accumulated in the celestial healpix sky pixels using the Fourier transform kernel:

$$e^{-2\pi(ul+vm+wn)} .$$

The Fourier transformation directly yields Stokes intensity vectors $[I, Q, U, V]^T$ in IAU frame.

Limiting errors at low elevations

All of the above measurement equations include a position-dependent correction for the dissimilar EEP beam patterns of the antennas in the station. The correction is made by effectively dividing the measured coherency vector by the beam response; therefore, in sky directions where the product of the complex beam patterns for a baseline is erroneously small, the baseline contributes a large spurious intensity. In the Fourier transform from baseline visibilities to sky intensities, the summation at any sky pixel might be dominated by anomalous contributions from a few such baselines, and avoidance of this imaging error requires an algorithm for rejecting such erroneous contributions.

The imaging process multiplies the coherency vector $[R_{XX}, R_{XY}, R_{YX}, R_{YY}]^T$ by the inverse of the matrix:

$$M = \left(\begin{bmatrix} B_{1X\phi} B_{1X\theta} \\ B_{1Y\phi} B_{1Y\theta} \end{bmatrix} \otimes \begin{bmatrix} B^*_{2X\phi} B^*_{2X\theta} \\ B^*_{2Y\phi} B^*_{2Y\theta} \end{bmatrix} \right) \begin{bmatrix} 1 & 1 & 0 & 0 \\ 0 & 0 & 1 & j \\ 0 & 0 & 1 & -j \\ 1 & -1 & 0 & 0 \end{bmatrix}$$

For each baseline and sky pixel, the inverse of matrix M is computed, the absolute values of the complex numbers in M^{-1} is evaluated, and the maximum of these is compared to a threshold. For the voltage beam patterns of AAVS2 station at 110 MHz, I have adopted a threshold that corresponds to rejecting pixel-baseline combinations where the beam response is less than 20%. The adopted algorithm requires careful revision and fine tuning if useful polarisation beam forming is to be done at low elevations below about 30 degrees.

I have prepared scripts that implement all three methods described above; unsurprisingly, for intra-station correlations of AAVS2, all three methods give identical Stokes images of the sky.

Example Stokes Images

I show below (in the following pages) images in Stokes I, Q, U and V made at UT 04 h, at a time close to when the Sun crossed the celestial meridian and was at its maximum elevation, and at UT 20 h, close to the time when the Galactic Centre was close to zenith.

The Stokes images presented here have not been deconvolved. Image intensities are in units of kelvin brightness. The images are "naturally" weighted, with all baselines given equal weights. Images are restricted to elevation angles above 30°. The healpix images were synthesised with NSIDE = 32, corresponding to pixels of 109.9 arcmin in size and providing a sampling of the sky of about two points per beam FWHM. The healpix images were then interpolated to a finer grid with NSIDE=128 for display.

The images are presented with a taper corresponding to the average embedded beam pattern and separately without any primary beam taper.

An example of the primary beam is shown below in Fig. 3 corresponding to the image made at UT 20h.

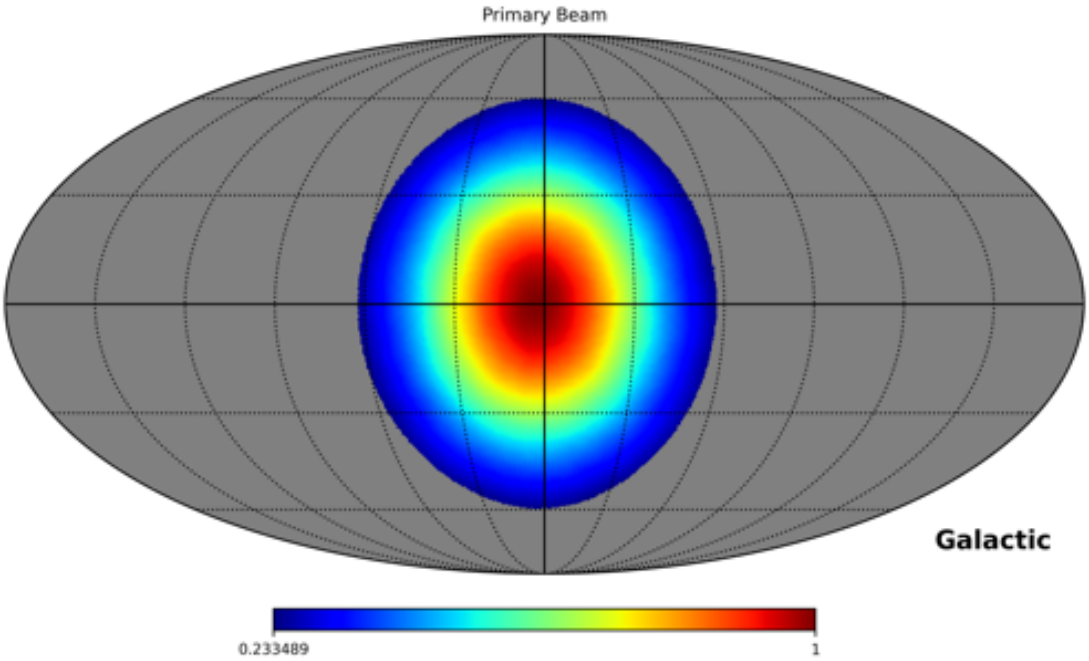

Figure 3 shows the primary beam for the image towards Galactic Centre, limited to elevations above 30 degrees. The image is in sky projection with North upwards, East to the left and zenith at the centre.

The primary beam response is at lowest 0.233 at elevation 30 degrees.

Figure 4: Stokes images made at 04 UT close to the time when the Sun crossed the celestial meridian. Images are limited to elevation angles above 30 degrees. Display of the all-sky healpix map is in Mollweide projection in equatorial coordinates. The image has been tapered with the average embedded beam pattern.

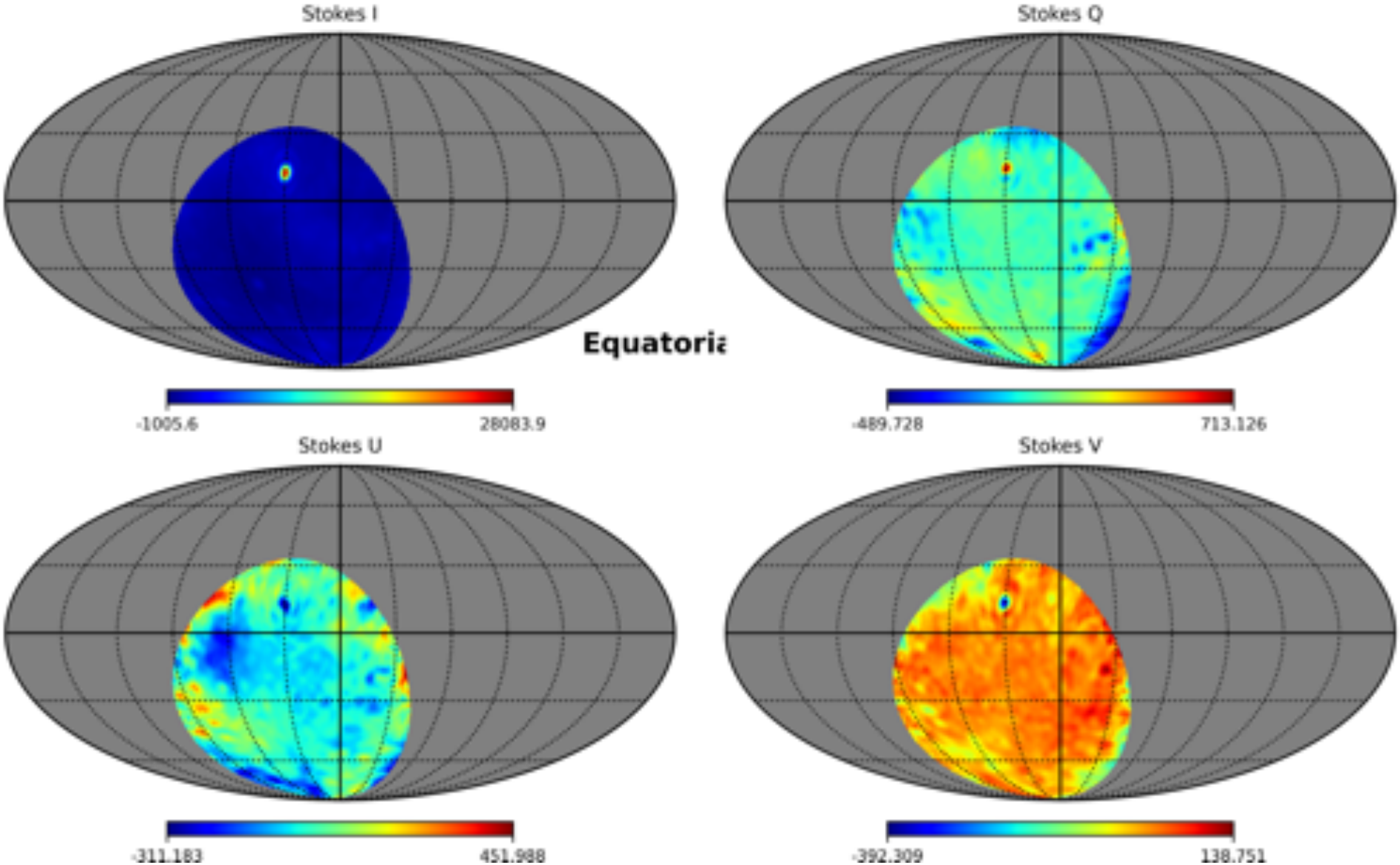

Figure 5: Stokes images made at 04 UT close to the time when the Sun crossed the celestial meridian. Images are limited to elevation angles above 30 degrees. Display of the all-sky healpix map is in Mollweide projection in equatorial coordinates.

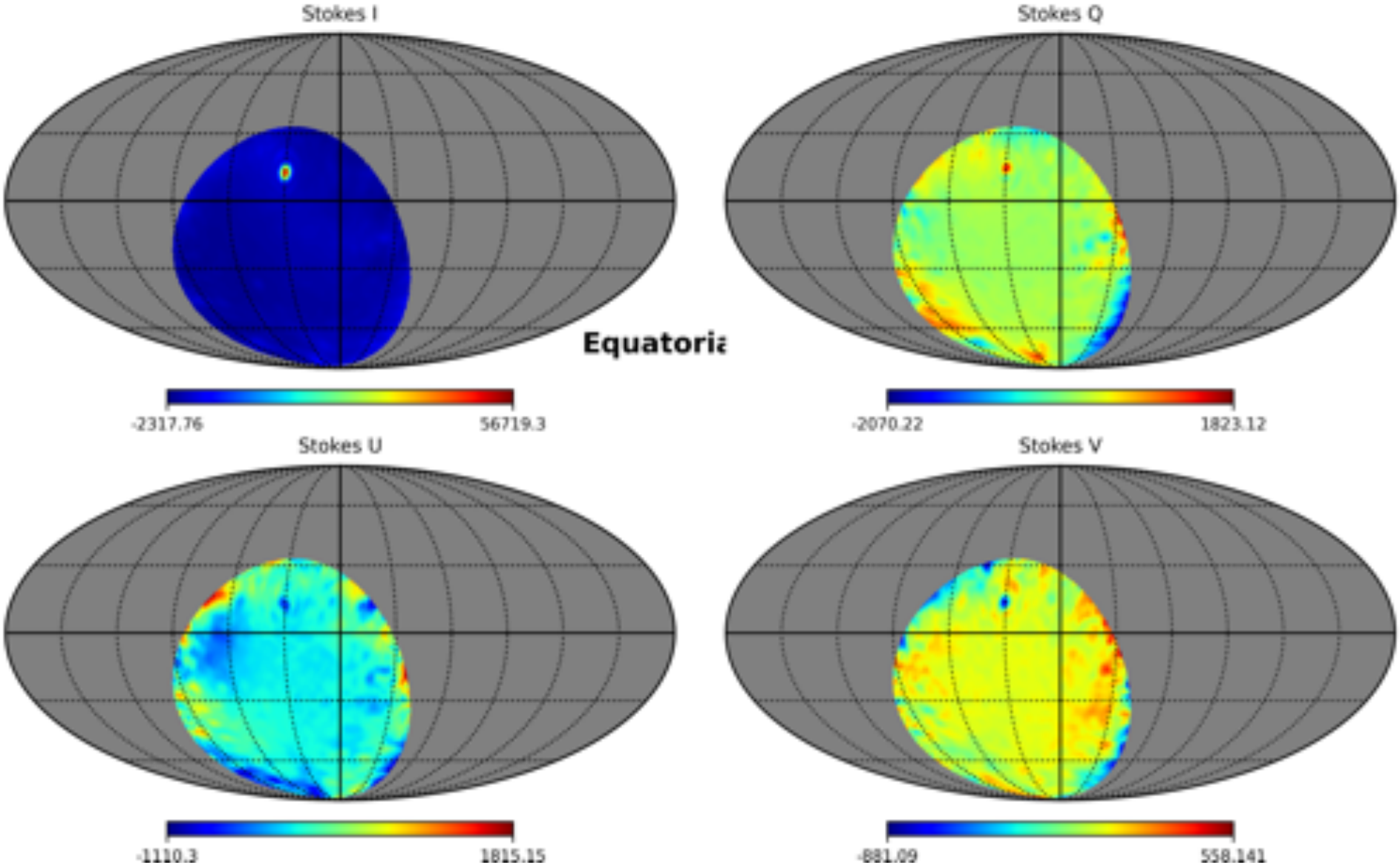

Figure 6: Stokes images made at 20 UT at about the time when the Galactic centre crossed the celestial meridian and was close to zenith at MRO. Images are limited to elevation angles above 30 degrees. Display of the all-sky healpix map is in Mollweide projection in Galactic coordinates. The image has been tapered with the average embedded beam pattern.

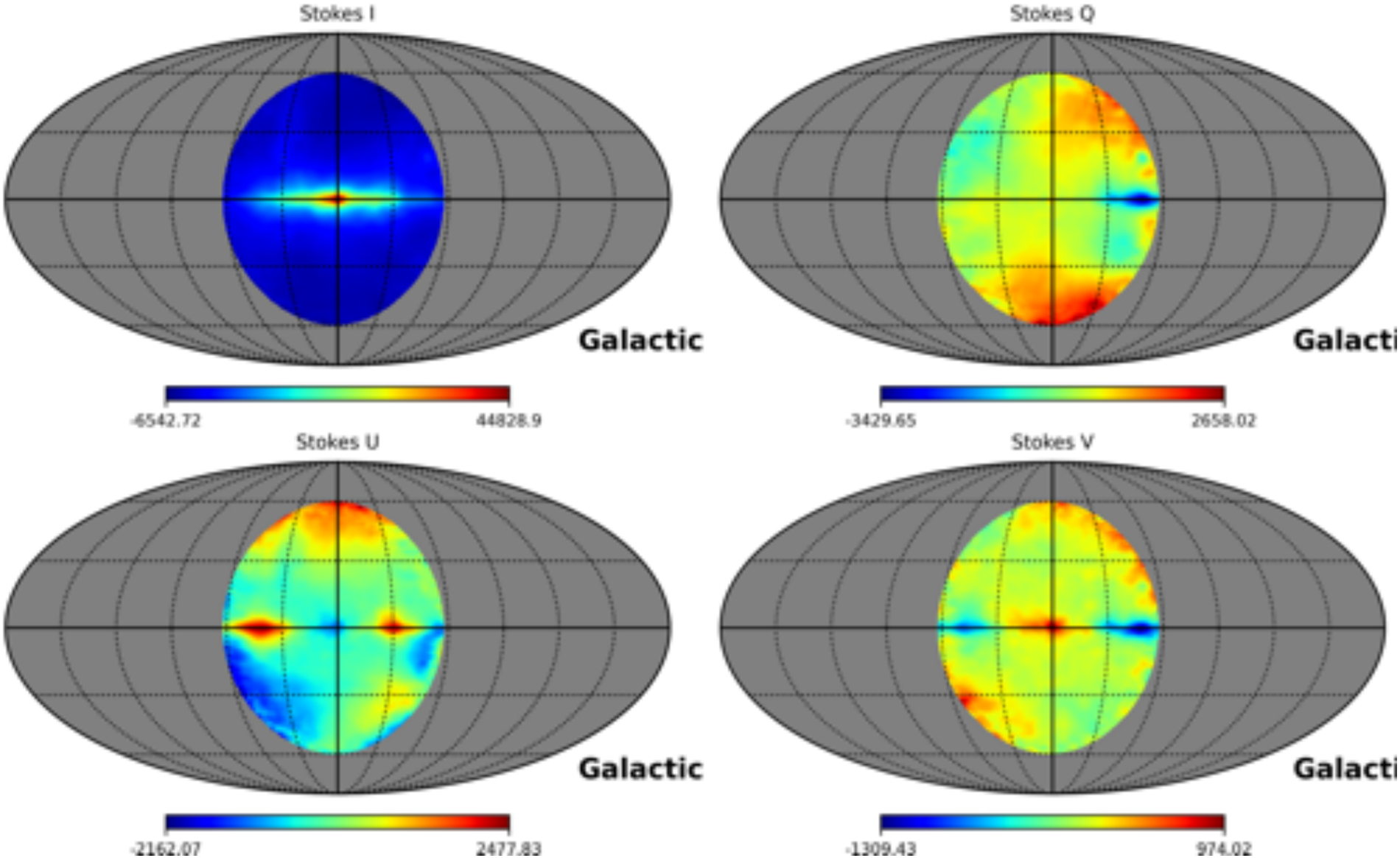

Figure 7: Stokes images made at 20 UT when the Galactic centre was close to zenith. Images are limited to elevation angles above 30 degrees. Display of the all-sky healpix map is in Mollweide projection in Galactic coordinates.

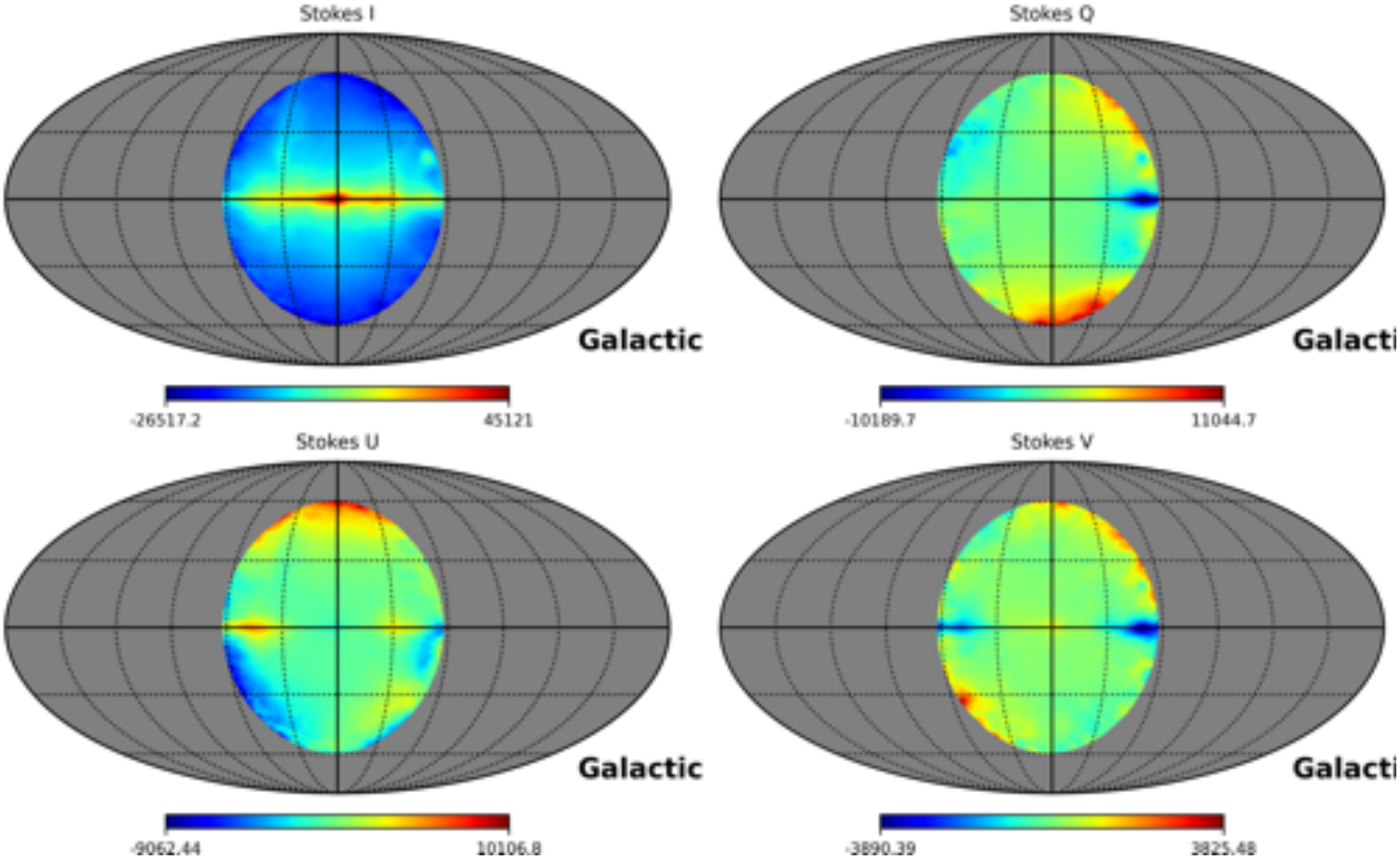

The pixel brightness towards the Sun, in the image with primary beam taper, is 28083, 632, -306 and -392 K in Stokes I, Q, U and V. Without this taper, the intensities are 56719, 1276, -618 and -792 K. The model of the Sun used for calibrating the visibility data had a pixel-averaged brightness temperature of 59466 K.

Towards the Galactic Centre, the Stokes I, Q, U and V intensities at the brightest pixel are 44828, 928, -885 and 974 K in the image with primary beam taper. In images without primary beam taper the corresponding Stokes intensities are 45121, 471, -944 and 855 K.

	I	Q	U	V	$\frac{\sqrt{Q^2+U^2}}{I}$	$\frac{\|V\|}{I}$
Sun (with PB taper)	28083	632	-306	-392	0.025	0.014
Sun (no PB taper)	56719	1276	-618	-792	0.025	0.014
GC (with PB taper	44828	928	-885	974	0.029	0.022
GC (no PB taper)	45121	471	-944	855	0.023	0.019

The fractional linear and circular polarisation is small towards the Sun and Galactic Centre, at transit and at high elevations. However, this is not the case off celestial meridian and at low elevations. I have examined the Stokes intensities towards the bright Galactic Centre, which transits overhead at MRO, at a set of hour angles:

GC at HA	AZ (deg)	EL (deg)	I	Q	U	V	$\frac{\sqrt{Q^2+U^2}}{I}$	$\frac{\|V\|}{I}$
-4h	108	39	62056	-16332	-11938	702	0.326	0.011
-2h	104	65	47705	-36	-260	123	0.006	0.003
0h	-152	86	45163	394	-953	835	0.023	0.018
2h	-100	62	48000	-1546	3805	122	0.086	0.003
4h	-110	36	64475	-24589	14947	-5943	0.446	0.092

And the Stokes intensities towards the Sun before and after meridian crossing show progressively increasing Stokes I, Q, U & V away from the crossing at UT 2h:

Sun at HA	AZ (deg)	EL (deg)	I	Q	U	V	$\frac{\sqrt{Q^2+U^2}}{I}$	$\frac{\|V\|}{I}$
-2h	42	40	68472	6150	35344	-8980	0.524	0.131
0h	3	50	59645	1419	-626	-816	0.026	0.014
2h	-38	42	71294	5158	-35784	6281	0.507	0.088